SIAM J. NUMER. ANAL.
Vol. 49, No. 3, pp. 1023–1045

CONSTRAINT PRESERVING SCHEMES USING POTENTIAL-BASED FLUXES. II. GENUINELY MULTIDIMENSIONAL SYSTEMS OF CONSERVATION LAWS*

SIDDHARTHA MISHRA† AND EITAN TADMOR‡

Abstract. We introduce a class of numerical schemes that preserve a discrete version of vorticity in conservation laws which involve grad advection. These schemes are based on reformulating finite volume schemes in terms of vertex centered *numerical potentials*. The resulting potential-based schemes have a genuinely multidimensional structure. A suitable choice of potentials leads to discrete vorticity preserving schemes that are simple to code, computationally inexpensive, and proven to be stable. We extend our discussion to other classes of genuinely multidimensional schemes. Numerical examples for linear grad advection equations, linear and nonlinear wave equation systems, and the Euler equations of gas dynamics are presented.

Key words. multidimensional evolution equations, nonlinear conservation laws, constraint transport, central difference schemes, potential-based fluxes

AMS subject classifications. 65M06, 35L65

DOI. 10.1137/090770138

1. Introduction—constraint transport.

We are concerned with hyperbolic systems of conservation laws in two space dimensions:

$$\mathbf{U}_t + \mathbf{f}(\mathbf{U})_x + \mathbf{g}(\mathbf{U})_y = 0, \quad (x, y, t) \in \mathbb{R} \times \mathbb{R} \times \mathbb{R}_+, \tag{1.1}$$

where $\mathbf{U}$ is the vector of unknowns and $\mathbf{f}, \mathbf{g}$ are the flux vectors in the x- and y-directions, respectively. Prototype examples for (1.1) include the Euler equations of gas dynamics, the shallow water equations of oceanography, the ideal magneto-hydrodynamics (MHD) equations of plasma physics and the equations of nonlinear elasticity.

It is well known that solutions of (1.1) develop discontinuities in the form of shock waves, even for smooth initial data. Hence, the solutions of (1.1) are sought in a weak sense. Weak solutions are not necessarily unique and (1.1) has to be supplemented with additional admissibility criteria, the so-called *entropy conditions* [8]. The existence and uniqueness theory for multidimensional single conservation laws and for some special cases of one-dimensional systems is well developed. A corresponding theory for multidimensional systems of conservation laws is still sought for.

1.1. Constraint transport.

Many physically relevant systems of conservation laws (1.1) are augmented with an *intrinsic* constraint. The MHD equations for plasma physics is a prototype model for such systems, whose solutions satisfy the constraint

*Received by the editors September 4, 2009; accepted for publication (in revised form) February 10, 2011; published electronically May 24, 2011.
http://www.siam.org/journals/sinum/49-3/77013.html
†Seminar for Applied Mathematics (SAM), ETH Zürich, Rämistrasse 101, Zürich-8092, Switzerland (smishra@sam.math.ethz.ch).
‡Department of Mathematics, Institute for Physical Science & Technology and Center of Scientific Computation and Mathematical Modeling (CSCAMM), University of Maryland, College Park, MD 20742 (tadmor@cscamm.umd.edu). This author's research was supported in part by NSF grants DMS07-07949, DMS10-08397, and ONR grant N00014-091-0385.

that the magnetic field remains divergence free [38]. Maintaining the div-free constraint in MHD computations is discussed in our subsequent work [24]. In this paper, we focus our attention on another closely related example, which involves the (dual) constraint of satisfying a *curl*-free condition. It consists of the general class of so-called *grad advection* equations of the form

$$\mathbf{U}_t + \nabla f(\mathbf{x}, t, \mathbf{U}) = 0, \quad (\mathbf{x}, t) \in \mathbb{R}^d \times \mathbb{R}_+. \tag{1.2}$$

Here, f is any scalar flux function and the vector of unknowns, $\mathbf{U}$, is sought subject to prescribed initial conditions, $\mathbf{U}(\cdot, 0) = \mathbf{U}_0(\cdot)$. Applying the curl operator to both sides of (1.2), we obtain that solutions of (1.2) satisfy the curl (vorticity) constraint,

$$\mathrm{curl}(\mathbf{U})_t \equiv 0. \tag{1.3}$$

In particular, the curl of the solution remains zero if $\mathrm{curl}(\mathbf{U}_0) \equiv 0$. Note that the above constraint holds true for any choice of the flux function f in (1.2). This is a dual problem for the curl advection problem whose div-free constraint transport was studied in [23].

We specify three concrete examples for such grad advection problems, (1.2). The first is a *linear* grad advection in two space dimensions,

$$\begin{aligned} (u_1)_t + (u_1 v_1 + u_2 v_2)_x &= 0, \\ (u_2)_t + (u_1 v_1 + u_2 v_2)_y &= 0. \end{aligned} \tag{1.4}$$

Here, $\mathbf{U} := (u_1, u_2)^\top$ is the unknown vector field and (1.4) models the grad advection under the action of an (smooth) external velocity field, $\mathbf{v} := (v_1, v_2)^\top$, and $\mathrm{curl}(\mathbf{U})$ amounts to the vorticity,

$$\omega := (u_2)_x - (u_1)_y, \tag{1.5}$$

which is preserved by the flow.

As a second example for a grad advection, (1.2), we consider the system of wave equations in two space dimensions [25]

$$\begin{aligned} p_t + (cu_1)_x + (cu_2)_y &= 0, \\ (u_1)_t + (cp)_x &= 0, \\ (u_2)_t + (cp)_y &= 0, \end{aligned} \tag{1.6}$$

where c is a given (constant) wave speed. The equations for $u_{1,2}$ in (1.6) have the special structure of the grad advection equation (1.2) with the flux $f = cp$. A straightforward calculation shows that the vorticity is preserved.

A related third example is the nonlinear wave equation (in two space dimensions),

$$p_{tt} - g(p)_{xx} - g(p)_{yy} = 0, \tag{1.7a}$$

where g is a nonlinear scalar function. The above equation can be recast as a first-order system yielding

$$\begin{aligned} p_t + (u_1)_x + (u_2)_y &= 0, \\ (u_1)_t + g(p)_x &= 0, \\ (u_2)_t + g(p)_y &= 0. \end{aligned} \tag{1.7b}$$

Again, the vorticity $\omega = (u_2)_x - (u_1)_y$ is preserved in the sense that $\omega_t \equiv 0$.

The system of wave equations and its nonlinear variant (1.7) have been introduced in [25] as prototypes for more complicated problems like the shallow water equations that involve a version of the vorticity constraint [16].

1.2. The discrete setup. Finite-volume (FV) methods are among the most widely used numerical methods for the approximate solution of systems of conservation laws such as (1.1); see [18, 35] and the references therein. In an FV approximation, the computational domain is discretized into cells and an integral form of the conservation law (1.1) is discretized on each cell. This method relies on constructing suitable numerical fluxes in the normal direction across each cell interface. For simplicity, we consider a uniform Cartesian mesh with mesh sizes $\Delta x, \Delta y$ in the x- and y-directions, respectively. It consists of the discrete cells, $\mathcal{C}_{i,j} := [x_{i-\frac{1}{2}}, x_{i+\frac{1}{2}}) \times [y_{j-\frac{1}{2}}, y_{j+\frac{1}{2}})$, centered at the mesh points $(x_i, y_j) = (i\Delta x, j\Delta y),\ (i,j) \in \mathbb{Z}^2$. The cell average of $\mathbf{U}$ over $\mathcal{C}_{i,j}$ (at time t), denoted as $\mathbf{U}_{i,j}(t)$, is updated with the semidiscrete scheme [18, 35],

$$\frac{d}{dt}\mathbf{U}_{\mathbf{i,j}} = -\frac{1}{\Delta x}\big(\mathbf{F}_{i+\frac{1}{2},j} - \mathbf{F}_{i-\frac{1}{2},j}\big) - \frac{1}{\Delta y}\big(\mathbf{G}_{i,j+\frac{1}{2}} - \mathbf{G}_{i,j-\frac{1}{2}}\big). \tag{1.8}$$

The time dependence of all the quantities in the above expression is suppressed for notational convenience. Classical first-order schemes employ two-point numerical fluxes of the form

$$\mathbf{F}_{i+\frac{1}{2},j} = \mathbf{F}(\mathbf{U}_{i,j}, \mathbf{U}_{i+1,j}), \quad \mathbf{G}_{i,j+\frac{1}{2}} = \mathbf{G}(\mathbf{U}_{i,j}, \mathbf{U}_{i,j+1}). \tag{1.9}$$

A canonical example is provided by the first-order Rusanov numerical flux:

$$\begin{aligned} \mathbf{F}_{i+\frac{1}{2},j} &= \frac{1}{2}\big(\mathbf{f}(\mathbf{U}_{i,j}) + \mathbf{f}(\mathbf{U}_{i+1,j})\big) - \max\{|(\alpha)_{i,j}|, |(\alpha)_{i+1,j}|\}\big(\mathbf{U}_{i+1,j} - \mathbf{U}_{i,j}\big), \\ \mathbf{G}_{i,j+\frac{1}{2}} &= \frac{1}{2}\big(\mathbf{g}(\mathbf{U}_{i,j}) + \mathbf{g}(\mathbf{U}_{i,j+1})\big) - \max\{|(\beta)_{i,j}|, |(\beta)_{i,j+1}|\}\big(\mathbf{U}_{i,j+1} - \mathbf{U}_{i,j}\big). \end{aligned} \tag{1.10}$$

Here, $\alpha_{i,j}$ and $\beta_{i,j}$ are the maximal eigenvalues of the Jacobians $\mathbf{A} = \partial_{\mathbf{U}}\mathbf{f}$ and $\mathbf{B} = \partial_{\mathbf{U}}\mathbf{g}$, respectively, for a given state $\mathbf{U}_{i,j}$:

$$\alpha_{i,j} := \operatorname{argmax}_\lambda\{|\lambda| : \lambda = \lambda\big(\mathbf{A}(\mathbf{U}_{\mathbf{i,j}})\big)\}, \quad \beta_{i,j} = \operatorname{argmax}_\lambda\{|\lambda| : \lambda = \lambda\big(\mathbf{B}(\mathbf{U}_{\mathbf{i,j}})\big)\}.$$

Note that the only characteristic information in the Rusanov flux is a local estimate on the wave speeds. This flux is almost Jacobian free, very simple to implement and has a very low computational cost. But its resolution is limited by the first-order accuracy. The first-order schemes (1.8), (1.9) can be extended to higher order accuracy by employing numerical fluxes based on wider, $2p$-point stencils, $I_{i+\frac{1}{2}} := \{i' \,\big|\, |i' - i - 1/2| < p\}$ along the x-axis and $J_{j+\frac{1}{2}} := \{j' \,\big|\, |j' - j - 1/2| < p\}$ along the y-axis,

$$\mathbf{F}_{i+\frac{1}{2},j} = \mathbf{F}\Big(\{\mathbf{U}_{i',j}\}_{i' \in I_{i+\frac{1}{2}}}\Big), \quad \mathbf{G}_{i,j+\frac{1}{2}} = \mathbf{G}\Big(\{\mathbf{U}_{i,j'}\}_{j' \in J_{j+\frac{1}{2}}}\Big). \tag{1.11}$$

The building blocks for such extensions are still the two-point numerical fluxes, $\mathbf{F}(\cdot,\cdot)$ and $\mathbf{G}(\cdot,\cdot)$. As a prototype example, we recall the class of second-order schemes based on piecewise bilinear MUSCL reconstruction [18]

$$\mathbf{p}_{i,j}(x,y) := \mathbf{U}_{i,j} + \frac{\mathbf{U}'_{i,j}}{\Delta x}(x - x_i) + \frac{\mathbf{U}^{\backprime}_{i,j}}{\Delta y}(y - y_j). \tag{1.12a}$$

Here, $\mathbf{U}'$ and $\mathbf{U}^{\backprime}$ denote the *numerical derivatives*

$$\begin{aligned} \mathbf{U}'_{i,j} &= \operatorname{minmod}\left(\mathbf{U}_{i+1,j} - \mathbf{U}_{i,j}, \frac{1}{2}(\mathbf{U}_{i+1,j} - \mathbf{U}_{i-1,j}), \mathbf{U}_{i,j} - \mathbf{U}_{i-1,j}\right), \\ \mathbf{U}^{\backprime}_{i,j} &= \operatorname{minmod}\left(\mathbf{U}_{i,j+1} - \mathbf{U}_{i,j}, \frac{1}{2}(\mathbf{U}_{i,j+1} - \mathbf{U}_{i,j-1}), \mathbf{U}_{i,j} - \mathbf{U}_{i,j-1}\right), \end{aligned} \tag{1.12b}$$

which utilize the minmod limiter

$$\text{(1.12c)}\quad \operatorname{minmod}(a,b,c)=\begin{cases} sgn(a)\min\{|a|,|b|,|c|\} & \text{if} \quad sgn(a)=sgn(b)=sgn(c),\\ 0 & \text{otherwise.}\end{cases}$$

In this manner, one can reconstruct in each cell $\mathcal{C}_{i,j}$ the point values

$$\text{(1.13a)}\qquad \begin{aligned} \mathbf{U}^E_{i,j}&:=\mathbf{p}_{i,j}(x_{i+\frac12},y_j), \quad \mathbf{U}^W_{i,j}:=\mathbf{p}_{i,j}(x_{i-\frac12},y_j),\\ \mathbf{U}^N_{i,j}&:=\mathbf{p}_{i,j}(x_i,y_{j+\frac12}), \quad \mathbf{U}^S_{i,j}:=\mathbf{p}_{i,j}(x_i,y_{j-\frac12}),\end{aligned}$$

from the given neighboring cell averages $\mathbf{U}_{i,j}$, $\mathbf{U}_{i\pm1,j}$, and $\mathbf{U}_{i,j}$, $\mathbf{U}_{i,j\pm1}$. The resulting second-order fluxes are then given by

$$\text{(1.13b)}\qquad \mathbf{F}_{i+\frac12,j}=\mathbf{F}(\mathbf{U}^E_{i,j},\mathbf{U}^W_{i+1,j}), \quad \mathbf{G}_{i,j+\frac12}=\mathbf{G}(\mathbf{U}^N_{i,j},\mathbf{U}^S_{i,j+1}).$$

The use of minmod limiter ensures the nonoscillatory behavior of the second-order schemes (1.8), (1.12). Observe that the second-order MUSCL fluxes (1.13b) are based on four-point stencils

$$\mathbf{F}_{i+\frac12,j}=\mathbf{F}(\mathbf{U}_{i-1,j},\mathbf{U}_{i,j},\mathbf{U}_{i+1,j},\mathbf{U}_{i+2,j}), \quad \mathbf{G}_{i,j+\frac12}=\mathbf{F}(\mathbf{U}_{i,j-1},\mathbf{U}_{i,j},\mathbf{U}_{i,j+1},\mathbf{U}_{i,j+2})$$

Similar reconstructions together with upwind or central averaging yield a large class of high-resolution FV semidiscrete schemes, e.g., [15, 30, 17], which could then be integrated in time using standard stable high-order Runge–Kutta methods [14].

1.3. Constraint transport in the discrete setup. Despite their considerable success, it is known that FV schemes could be deficient in resolving genuinely multidimensional waves in the solution of (1.1) [18]. Equations which are bound by the curl- and div-free constraints, for example, involve the *geometric* interaction of both normal and transverse components of the solution: they reflect the genuinely multidimensional structure of (1.1). Standard FV fluxes, $\mathbf{F}_{i+\frac12,j},\mathbf{G}_{i,j+\frac12}$, (1.11), which are supported along normal directions of the x- and y-axis but otherwise *lack explicit transverse information*, could result in poor approximation of these genuinely multidimensional waves [38]. Considerable effort has been devoted to devising FV schemes for (1.1), which respect its associated transported constraints. Examples of genuinely multidimensional (GMD) schemes include dimensional splitting [18], the corner transport upwind method [7] (see also [4]), wave propagation based on solving transverse Riemann problems [18], the method of transport [11, 12, 27], the FV evolution Galerkin methods [20, 21], and the residual distribution (fluctuation splitting) schemes on unstructured meshes designed in [10, 1, 26]. Examples of GMD schemes that are adapted to preserve constraints include the projection methods [5, 6], methods that add source terms [28, 13], and constraint transport methods based on staggering [3, 9, 16, 25, 29, 36, 37, 2]. These methods are compared extensively in [38].

The absence of an optimal strategy for discretizing constraint transport problems leaves room for designing stable GMD schemes which are (i) easy to formulate and code; (ii) have a low computational cost; and (iii) preserve constraint(s) properties rendered by the multidimensional structure of the system (1.1). Their numerical fluxes take a general form

$$\text{(1.14a)}\qquad \mathbf{F}_{i+\frac12,j}=\mathbf{F}\left(\left\{\mathbf{U}_{(i',j')\in S_{i+\frac12,j}}\right\}\right), \quad \mathbf{G}_{i,j+\frac12}=\mathbf{G}\left(\left\{\mathbf{U}_{(i',j')\in S_{i,j+\frac12}}\right\}\right).$$

Here, $S_{i+\frac{1}{2},j}$ and $S_{i,j+\frac{1}{2}}$ are *GMD* stencils which, in contrast to (1.11), allow us to incorporate information from both the normal and transverse directions,

$$S_{i+\frac{1}{2},j} := \big\{(i',j') \,\big|\, |i'-i-1/2|+|j'-j|<q\big\},$$
$$S_{i,j+\frac{1}{2}} := \big\{(i',j') \,\big|\, |i'-i|+|j'-j-1/2|<q\big\}. \tag{1.14b}$$

The *primary aim* of this paper is to design numerical schemes for the class of grad advection problems (1.2) which preserve a discrete version of the vorticity constraint (1.3). We follow the approach of a recent paper [23] and rewrite the edge centered numerical fluxes in the standard FV formulation (1.8) in terms of vertex centered *numerical potentials*. We show that the family of such potentials is rich, and that a suitable choice of these numerical potentials allows us to preserve a discrete version of the vorticity constraint. In this context, we consider the linear grad advection (1.4) and the system wave equation (1.6) in detail and elaborate the potential-based constraint preserving schemes. These schemes are shown to be energy stable for the system wave equation. The potential-based schemes motivates our *second aim* in this paper, namely, the study of GMD discretizations for general conservation laws which are not necessarily limited by a transport constraint.

The rest of this paper is organized as follows. In section 2 we introduce different classes of potential-based schemes for general two-dimensional conservation laws, (1.1). In section 3 we focus our attention on the grad advection problems and related system wave equation: we show that suitable choices of numerical potentials for the grad advection problems lead to vorticity preserving schemes, and we prove the L^2-stability of these schemes for the system wave equation. Numerical experiments for the vorticity preserving schemes are presented in section 4. The reformulation of FV schemes in terms of vertex centered numerical potentials leads to the incorporation of explicit transverse information, and it is responsible for the GMD features for the class of potential-based FV schemes. Finally, motivated by these features of the potential-based schemes, we introduce, in section 5, a related class of GMD FV schemes. Their GMD character, outlined in section 5.1, is built-in by differencing along transverse *and* diagonal directions across each cell. In section 5.2 we prove the entropy stability of this new class of so-called *isotropic schemes* for general two-dimensional conservation laws. Indeed, general systems of conservation laws are not necessarily limited by any constraint transport, and it is therefore natural to examine the performance of GMD schemes on nonlinear problems without intrinsic constraints. We explore this issue in section 5.3, investigating the performance of these isotropic schemes, via numerical experiments with the two-dimensional Euler equations of gas dynamics.

2. Potential-based schemes. The design of potential-based schemes for general two-dimensional conservation laws (1.1) involves *numerical potentials* $\phi = \phi_{i+\frac{1}{2},j+\frac{1}{2}}$ and $\psi = \psi_{i+\frac{1}{2},j+\frac{1}{2}}$ at each vertex $(x_{i+\frac{1}{2}}, y_{j+\frac{1}{2}})$, with the sole requirement that these potentials be consistent with the differential fluxes, i.e.,

$$\phi_{i+\frac{1}{2},j+\frac{1}{2}}(\mathbf{U},\dots,\mathbf{U}) = \mathbf{f}(\mathbf{U}), \quad \psi_{i+\frac{1}{2},j+\frac{1}{2}}(\mathbf{U},\dots,\mathbf{U}) = \mathbf{g}(\mathbf{U}).$$

Given the numerical potentials, ϕ, ψ, we now set the corresponding numerical fluxes,

$$\mathbf{F}_{i+\frac{1}{2},j} = \mu_y \phi_{i+\frac{1}{2},j},$$
$$\mathbf{G}_{i,j+\frac{1}{2}} = \mu_x \psi_{i,j+\frac{1}{2}}. \tag{2.1}$$

The resulting FV scheme written in terms of these numerical potentials reads

$$\begin{aligned}\frac{d}{dt}\mathbf{U}_{i,j} &= -\frac{1}{\Delta x}\delta_x\mu_y\phi_{i,j} - \frac{1}{\Delta y}\delta_y\mu_x\psi_{i,j},\\ &= -\frac{1}{\Delta x}\left(\frac{1}{2}(\phi_{i+\frac{1}{2},j+\frac{1}{2}} + \phi_{i+\frac{1}{2},j-\frac{1}{2}}) - \frac{1}{2}(\phi_{i-\frac{1}{2},j+\frac{1}{2}} + \phi_{i-\frac{1}{2},j-\frac{1}{2}})\right)\\ &\quad - \frac{1}{\Delta y}\left(\frac{1}{2}(\psi_{i+\frac{1}{2},j+\frac{1}{2}} + \psi_{i-\frac{1}{2},j+\frac{1}{2}}) - \frac{1}{2}(\psi_{i+\frac{1}{2},j-\frac{1}{2}} + \psi_{i-\frac{1}{2},j-\frac{1}{2}})\right).\end{aligned} \tag{2.2}$$

Remark 2.1. Throughout this paper, we use the following standard notation for averaging and (undivided) differencing:

$$\begin{aligned}\mu_x a_{I,J} &:= \frac{a_{I+\frac{1}{2},J} + a_{I-\frac{1}{2},J}}{2}, \quad \mu_y a_{I,J} := \frac{a_{I,J+\frac{1}{2}} + a_{I,J-\frac{1}{2}}}{2},\\ \delta_x a_{I,J} &:= a_{I+\frac{1}{2},J} - a_{I-\frac{1}{2},J}, \quad \delta_y a_{I,J} := a_{I,J+\frac{1}{2}} - a_{I,J-\frac{1}{2}}.\end{aligned} \tag{2.3}$$

We note that the above discrete operators could be used with indexes I, J which are placed at the center or at the edge of the computational cells, e.g., $I = i$ or $I = i + \frac{1}{2}$. In either case, we tag the resulting discrete operators according to the center of their stencil; thus, for example, $\mu_x w_{i+\frac{1}{2}}$ employs grid values placed on the integer-indexed edges, w_i and w_{i+1}, whereas $\delta_y w_j$ employs the half-integer indexed centers, $w_{j\pm\frac{1}{2}}$.

The potential-based scheme (2.2) is clearly conservative, as well as consistent since the potentials, ϕ and ψ, are consistent. The genuinely multidimensional nature of the scheme is evident from (2.2): the potentials are differenced in the normal direction but averaged in the transverse direction. We claim that the family of potential-based schemes (2.2) is *rich*: any standard FV flux can be used as a building block for constructing the numerical potentials in (2.1), and the resulting potential-based scheme inherits the accuracy of the underlying numerical flux. There are several ways to pursue the construction of numerical potentials and we outline two of them below; consult [23].

2.1. Symmetric potentials. In this approach, the potentials are defined by averaging the FV fluxes neighboring a vertex:

$$\begin{aligned}\phi_{i+\frac{1}{2},j+\frac{1}{2}} &= \mu_y\mathbf{F}_{i+\frac{1}{2},j+\frac{1}{2}},\\ \psi_{i+\frac{1}{2},j+\frac{1}{2}} &= \mu_x\mathbf{G}_{i+\frac{1}{2},j+\frac{1}{2}},\end{aligned} \tag{2.4}$$

where $\mathbf{F}, \mathbf{G}$ are any numerical fluxes consistent with $\mathbf{f}$ and $\mathbf{g}$, respectively. An explicit computation of (2.2) with potentials (2.4) leads to the revealing form

$$\begin{aligned}\frac{d}{dt}\mathbf{U}_{i,j} = &-\frac{1}{2\Delta x}(\mu_y\mathbf{F}_{i+\frac{1}{2},j+\frac{1}{2}} + \mu_y\mathbf{F}_{i+\frac{1}{2},j-\frac{1}{2}} - \mu_y\mathbf{F}_{i-\frac{1}{2},j+\frac{1}{2}} - \mu_y\mathbf{F}_{i-\frac{1}{2},j-\frac{1}{2}})\\ &- \frac{1}{2\Delta y}(\mu_x\mathbf{G}_{i+\frac{1}{2},j+\frac{1}{2}} + \mu_x\mathbf{G}_{i-\frac{1}{2},j+\frac{1}{2}} - \mu_x\mathbf{G}_{i+\frac{1}{2},j-\frac{1}{2}} - \mu_x\mathbf{G}_{i-\frac{1}{2},j-\frac{1}{2}}).\end{aligned} \tag{2.5}$$

Comparing the potential-based scheme (2.5) with the standard FV scheme (1.8), we observe that the former modifies (1.8) by averaging the fluxes in the transverse direction. Hence, it incorporates *explicit* transverse information in each direction. When employing two-point fluxes, the local stencil for the potential-based scheme (2.5) consists of nine points instead of the five-point stencil for the standard FV scheme (1.8). One can use wider stencils to achieve higher order of accuracy; for example, the symmetric potential-based scheme based on second-order four-point MUSCL flux (1.12) yields a second-order scheme based on a stencil of twenty-three points.

2.2. Diagonal potentials. We define the diagonal potentials [23],

$$\begin{aligned}\phi_{i+\frac{1}{2},j+\frac{1}{2}} &= \frac{1}{2}\left(\mathbf{F}^{+}_{i+\frac{1}{2},j+\frac{1}{2}} + \mathbf{F}^{-}_{i+\frac{1}{2},j+\frac{1}{2}}\right),\\ \psi_{i+\frac{1}{2},j+\frac{1}{2}} &= \frac{1}{2}\left(\mathbf{G}^{+}_{i+\frac{1}{2},j+\frac{1}{2}} + \mathbf{G}^{-}_{i+\frac{1}{2},j+\frac{1}{2}}\right).\end{aligned} \tag{2.6a}$$

Here, $\mathbf{F}^{\pm}, \mathbf{G}^{\pm}$ are the *diagonal* fluxes

$$\begin{aligned}\mathbf{F}^{+}_{i+\frac{1}{2},j+\frac{1}{2}} &:= \mathbf{F}(\mathbf{U}_{i,j}, \mathbf{U}_{i+1,j+1}), \quad \mathbf{F}^{-}_{i+\frac{1}{2},j+\frac{1}{2}} = \mathbf{F}(\mathbf{U}_{i,j+1}, \mathbf{U}_{i+1,j}),\\ \mathbf{G}^{+}_{i+\frac{1}{2},j+\frac{1}{2}} &:= \mathbf{G}(\mathbf{U}_{i,j}, \mathbf{U}_{i+1,j+1}), \quad \mathbf{G}^{-}_{i+\frac{1}{2},j+\frac{1}{2}} := \mathbf{G}(\mathbf{U}_{i+1,j}, \mathbf{U}_{i,j+1})\end{aligned} \tag{2.6b}$$

which amount to rotating the x- and y-axes by angles of $\frac{\pi}{4}$ and $-\frac{\pi}{4}$, where $\mathbf{F}(\cdot,\cdot)$ and $\mathbf{G}(\cdot,\cdot)$ are any two-point numerical fluxes consistent with $\mathbf{f}$ and $\mathbf{g}$.

3. Vorticity preserving schemes.

3.1. Vorticity preserving schemes for linear grad advection. For the sake of simplicity, we consider the family of grad advection equations (1.2) in two space dimensions:

$$\begin{aligned}(u_1)_t + f_x &= 0,\\ (u_2)_t + f_y &= 0.\end{aligned} \tag{3.1}$$

Here, $f = f(\mathbf{x}, t, u_1, u_2)$ is any scalar flux function. Equation (1.2) can be written as a two-dimensional conservation law (1.1) with

$$\mathbf{U} = (u_1, u_2)^{\top}, \quad \mathbf{f} = (f, 0)^{\top}, \quad \text{and} \quad \mathbf{g} = (0, f)^{\top}. \tag{3.2}$$

The class of potential-based schemes (2.1) is now readily available to be used with the appropriate potentials, ϕ, ψ, which reflect the special character of the fluxes $\mathbf{f} = (f, 0)^{\top}$ and $\mathbf{g} = (0, f)^{\top}$,

$$\begin{aligned}\phi_{i+1/2,j+1/2} &= \left(\chi_{i+1/2,j+1/2}, 0\right)^{\top},\\ \psi_{i+1/2,j+1/2} &= \left(0, \chi_{i+1/2,j+1/2}\right)^{\top}.\end{aligned} \tag{3.3}$$

Here, χ is *any* scalar numerical potential consistent with flux f in (3.1). The resulting potential-based scheme (2.2) now reads

$$\begin{aligned}\frac{d}{dt}(u_1)_{i,j} &= -\frac{1}{\Delta x}\delta_x \mu_y \chi_{i,j},\\ \frac{d}{dt}(u_2)_{i,j} &= -\frac{1}{\Delta y}\delta_y \mu_x \chi_{i,j}.\end{aligned} \tag{3.4}$$

The constraint preserving property for this class of potential-based schemes is summarized below.

LEMMA 3.1. *Let $(u_1)_{i,j}, (u_2)_{i,j}$ be the approximate solutions of* (3.1)*, computed with the potential-based scheme* (3.4)*. Then the discrete vorticity, ω^*,*

$$\omega^*_{i,j} := \frac{1}{\Delta x}(\mu_y \delta_x (u_2)_{i,j}) - \frac{1}{\Delta y}(\mu_x \delta_y (u_1)_{i,j}), \tag{3.5a}$$

is preserved in time,

$$\frac{d}{dt}(\omega^*_{i,j}) = 0 \quad \forall i,j. \tag{3.5b}$$

Verification of (3.5) is straightforward: since the difference operators δ_x, δ_y and the averaging operators μ_x, μ_y commute with each other, we may use (3.4) to find

$$\frac{d}{dt}\omega^*_{i,j} = -(\mu_y\delta_x\delta_y\mu_x - \mu_x\delta_y\delta_x\mu_y)\chi_{i,j} \equiv 0.$$

Remark 3.1. One approach in designing constraint preserving schemes is to satisfy that constraint *approximately*. For example, a discrete statement of the vorticity constraint could be interpreted as a second-order approximation of the differential vorticity, $\omega^*_{i,j} = \omega(x_i, y_j) + \mathcal{O}(\Delta x^2 + \Delta y^2)$. This, however, requires the smoothness of the underlying solution. Instead, a key feature of constraint preserving schemes based on numerical potentials is that they satisfy *exactly* a discrete constraint, so that their numerical solution remains on a discrete submanifold, independent of the underlying smoothness.

The above result holds for *any* consistent choice of the numerical potential χ. We outline the two specific choices of numerical potentials outlined in section 2.

(i) Vorticity preserving symmetric scheme. We choose χ to be the symmetric potential

$$\chi_{i+\frac{1}{2},j+\frac{1}{2}} = \frac{1}{4}\Big((\mathbf{F}_1)_{i+\frac{1}{2},j} + (\mathbf{F}_1)_{i+\frac{1}{2},j+1} + (\mathbf{G}_2)_{i,j+\frac{1}{2}} + (\mathbf{G}_2)_{i+1,j+\frac{1}{2}}\Big). \tag{3.6}$$

The numerical fluxes $\mathbf{F} = (\mathbf{F}_1, \mathbf{F}_2)^\top$ and $\mathbf{G} = (\mathbf{G}_1, \mathbf{G}_2)^\top$ are given by the Rusanov flux (1.10) for (3.1). The scheme (3.4) with the symmetric potential (3.6) is termed as the vorticity preserving symmetric scheme.

(ii) Vorticity preserving diagonal scheme. We choose χ to be the diagonal potential

$$\chi_{i+\frac{1}{2},j+\frac{1}{2}} = \frac{1}{4}\Big((\mathbf{F}_1^+)_{i+\frac{1}{2},j+\frac{1}{2}} + (\mathbf{F}_1^-)_{i+\frac{1}{2},j+\frac{1}{2}} + (\mathbf{G}_2^+)_{i+\frac{1}{2},j+\frac{1}{2}} + (\mathbf{G}_2^-)_{i+\frac{1}{2},j+\frac{1}{2}}\Big). \tag{3.7}$$

The diagonal fluxes $\mathbf{F}^\pm = \big(\mathbf{F}_1^\pm, \mathbf{F}_2^\pm\big)^\top$ and $\mathbf{G}^\pm = \big(\mathbf{G}_1^\pm, \mathbf{G}_2^\pm\big)^\top$ are given by the formula (2.6b) based on the Rusanov flux (1.10) for (3.1). The scheme (3.4) with the diagonal potential (3.7) is termed as the vorticity preserving diagonal scheme.

3.2. Vorticity preserving schemes for the system wave equation. We elaborate the vorticity preserving schemes of the previous section for the system wave equation (1.6). For simplicity, we focus on the symmetric vorticity preserving scheme (we refer here to the earlier study of Morton and Roe [25]). Note that the system wave equation (1.6) consists of two coupled parts: the velocity field (u_1, u_2) is governed by grad advection equation of the type (3.1) with a flux $f = cp$, which is coupled to a transport equation for the pressure p, with x-axis and y-axis fluxes, cu_1 and, respectively, cu_2. The symmetric potential-based scheme for the system wave equation (1.6) combines the scheme (3.4) (with symmetric potential (3.6)) with a symmetric potential-based scheme (2.5) for the pressure equation in (1.6).

Writing the system wave equation (1.6) as a two-dimensional conservation law (1.1),

$$\mathbf{U} = (p, u_1, u_2)^\top, \quad \mathbf{f} = (cu_1, cp, 0)^\top, \quad \text{and} \quad \mathbf{g} = (cu_2, 0, cp)^\top, \tag{3.8}$$

we choose the numerical potential

(3.9)
$$\phi_{i+\frac{1}{2},j+\frac{1}{2}} = \Big((\phi_1)_{i+\frac{1}{2},j+\frac{1}{2}}, \chi_{i+\frac{1}{2},j+\frac{1}{2}}, 0\Big)^\top, \quad \psi_{i+\frac{1}{2},j+\frac{1}{2}} = \Big((\psi_1)_{i+\frac{1}{2},j+\frac{1}{2}}, 0, \chi_{i+\frac{1}{2},j+\frac{1}{2}}\Big)^\top.$$

The components ϕ_1, ψ_1 are consistent with the fluxes $\mathbf{f}_1 = cu_1$ and $\mathbf{g}_1 = cu_2$, respectively. The potential χ can be chosen as the symmetric potential

$$\chi_{i+\frac{1}{2},j+\frac{1}{2}} = \frac{1}{4}\Big((\mathbf{F}_2)_{i+\frac{1}{2},j} + (\mathbf{F}_2)_{i+\frac{1}{2},j+1} + (\mathbf{G}_3)_{i,j+\frac{1}{2}} + (\mathbf{G}_3)_{i+1,j+\frac{1}{2}}\Big). \tag{3.10}$$

The numerical fluxes $\mathbf{F}_2, \mathbf{G}_3$ are the corresponding components of the Rusanov flux (1.10) for (1.6). The resulting potential based scheme reads as

$$\begin{aligned}
\frac{d}{dt}p_{i,j} &= -\frac{1}{\Delta x}\delta_x\mu_y(\phi_1)_{i,j} - \frac{1}{\Delta y}\delta_y\mu_x(\psi_1)_{i,j},\\
\frac{d}{dt}(u_1)_{i,j} &= -\frac{1}{\Delta x}\delta_x\mu_y\chi_{i,j},\\
\frac{d}{dt}(u_2)_{i,j} &= -\frac{1}{\Delta y}\delta_y\mu_x\chi_{i,j}.
\end{aligned} \tag{3.11}$$

Substituting the explicit formulas for the potentials and the Rusanov flux in (3.11), we obtain the following explicit form of this scheme:

$$\begin{aligned}
\frac{d}{dt}p_{i,j} &= -\frac{c}{4}D_{0x}\Big((u_1)_{i,j+1} + 2(u_1)_{i,j} + (u_1)_{i,j-1}\Big)\\
&\quad - \frac{c}{4}D_{0y}\Big((u_2)_{i+1,j} + 2(u_2)_{i,j} + (u_2)_{i-1,j}\Big)\\
&\quad + \frac{|c|\Delta x}{8}D_{+x}D_{-x}\Big(p_{i,j+1} + 2p_{i,j} + p_{i,j-1}\Big)\\
&\quad + \frac{|c|\Delta y}{8}D_{+y}D_{-y}\Big(p_{i+1,j} + 2p_{i,j} + p_{i-1,j}\Big),\\
\frac{d}{dt}(u_1)_{ij} &= -\frac{c}{4}D_{0x}\Big(p_{i,j+1} + 2p_{i,j} + p_{i,j-1}\Big)\\
&\quad + \frac{|c|\Delta x}{8}D_{+x}D_{-x}\Big((u_1)_{i,j+1} + 2(u_1)_{i,j} + (u_1)_{i,j-1}\Big)\\
&\quad + \frac{|c|\Delta y}{8}D_{+y}D_{-y}\Big((u_1)_{i+1,j} + 2(u_1)_{i,j} + (u_1)_{i-1,j}\Big),\\
\frac{d}{dt}(u_2)_{ij} &= -\frac{c}{4}D_{0y}\Big(p_{i+1,j} + 2p_{i,j} + p_{i-1,j}\Big)\\
&\quad + \frac{|c|\Delta x}{8}D_{+x}D_{-x}\Big((u_2)_{i,j+1} + 2(u_2)_{i,j} + (u_2)_{i,j-1}\Big)\\
&\quad + \frac{|c|\Delta y}{8}D_{+y}D_{-y}\Big((u_2)_{i+1,j} + 2(u_2)_{i,j} + (u_2)_{i-1,j}\Big).
\end{aligned} \tag{3.12}$$

Here we use the standard notation for divided differences, e.g.,

$$\begin{aligned}
D_{\pm x}a_{i,j} &= \pm\frac{a_{i\pm1,j} - a_{i,j}}{\Delta x}, \quad D_{0x}a_{i,j} = \frac{1}{2\Delta x}\left(a_{i+1,j} - a_{i-1,j}\right),\\
D_{+y}D_{-y}a_{i,j} &= \frac{1}{(\Delta y)^2}\left(a_{i,j+1} - 2a_{i,j} + a_{i,j-1}\right).
\end{aligned}$$

3.2.1. Stability analysis. We show that the above scheme (3.11) is L^2-energy stable.

THEOREM 3.2. *Let $p_{i,j}, (u_1)_{i,j}$, and $(u_2)_{i,j}$ be the approximate solutions of the system wave equation* (1.6)*, generated by the vorticity preserving symmetric scheme* (3.12)*. We assume that $p_{i,j}, (u_1)_{i,j}, (u_2)_{i,j} \to 0$ as $|i|, |j| \to \infty$. Let the discrete energy be*

$$\mathcal{E}_{i,j}(t) := \frac{1}{2}\left(p^2_{i,j}(t) + (u_1)^2_{i,j}(t) + (u_2)^2_{i,j}(t)\right); \tag{3.13}$$

then the approximations satisfy the discrete energy bound,

$$\sum_{i,j} \Delta x \Delta y \mathcal{E}_{i,j}(T) \leq \sum_{i,j} \Delta x \Delta y \mathcal{E}_{i,j}(0) \quad \forall T > 0. \tag{3.14}$$

Proof. We drop the t dependence of all quantities for notational convenience and denote

$$\begin{aligned}
&\widehat{H}_{i+\frac{1}{2},j+\frac{1}{2}} = p_{i,j}(u_1)_{i+1,j+1}, \quad H_{i+\frac{1}{2},j} = p_{i,j}(u_1)_{i+1,j}, \quad \widetilde{H}_{i+\frac{1}{2},j-\frac{1}{2}} = p_{i,j}(u_1)_{i+1,j-1},\\
&\widehat{K}_{i-\frac{1}{2},j-\frac{1}{2}} = p_{i,j}(u_1)_{i-1,j-1}, \quad K_{i-\frac{1}{2},j} = p_{i,j}(u_1)_{i-1,j}, \quad \widetilde{K}_{i-\frac{1}{2},j+\frac{1}{2}} = p_{i,j}(u_1)_{i-1,j+1},\\
&\widehat{L}_{i+\frac{1}{2},j+\frac{1}{2}} = p_{i,j}(u_2)_{i+1,j+1}, \quad L_{i,j+\frac{1}{2}} = p_{i,j}(u_2)_{i,j+1}, \quad \widetilde{L}_{i-\frac{1}{2},j+\frac{1}{2}} = p_{i,j}(u_2)_{i-1,j+1},\\
&\widehat{M}_{i-\frac{1}{2},j-\frac{1}{2}} = p_{i,j}(u_2)_{i-1,j-1}, \quad M_{i,j-\frac{1}{2}} = p_{i,j}(u_2)_{i,j-1}, \quad \widetilde{M}_{i+\frac{1}{2},j-\frac{1}{2}} = p_{i,j}(u_2)_{i+1,j-1}.
\end{aligned}$$

Multiplying both sides of (3.12) with $(p_{i,j}, (u_1)_{i,j}, (u_2)_{i,j})^\top$ and summing the three components, we obtain using the definition of discrete energy that

$$\frac{d}{dt}\sum_{i,j} \mathcal{E}_{i,j}(t) = \mathcal{T}_1 + \mathcal{T}_2. \tag{3.15}$$

Here, $\mathcal{T}_1$ is given by

(3.16)

$$\begin{aligned}
\mathcal{T}_1 := &-\frac{c}{8\Delta x}\sum_{i,j}\left(\widehat{H}_{i+\frac{1}{2},j+\frac{1}{2}} + H_{i+\frac{1}{2},j} + \widetilde{H}_{i+\frac{1}{2},j-\frac{1}{2}} - \widetilde{K}_{i-\frac{1}{2},j+\frac{1}{2}} - K_{i-\frac{1}{2},j} - \widehat{K}_{i-\frac{1}{2},j-\frac{1}{2}}\right)\\
&-\frac{c}{8\Delta y}\sum_{i,j}\left(\widehat{L}_{i+\frac{1}{2},j+\frac{1}{2}} + L_{i+\frac{1}{2},j} + \widetilde{L}_{i+\frac{1}{2},j-\frac{1}{2}} - \widetilde{M}_{i-\frac{1}{2},j+\frac{1}{2}} - M_{i-\frac{1}{2},j} - \widehat{M}_{i-\frac{1}{2},j-\frac{1}{2}}\right)\\
&-\frac{c}{8\Delta x}\sum_{i,j}\left(\widehat{K}_{i+\frac{1}{2},j+\frac{1}{2}} + K_{i+\frac{1}{2},j} + \widetilde{K}_{i+\frac{1}{2},j-\frac{1}{2}} - \widetilde{H}_{i-\frac{1}{2},j+\frac{1}{2}} - H_{i-\frac{1}{2},j} - \widehat{H}_{i-\frac{1}{2},j-\frac{1}{2}}\right)\\
&-\frac{c}{8\Delta y}\sum_{i,j}\left(\widehat{M}_{i+\frac{1}{2},j+\frac{1}{2}} + M_{i+\frac{1}{2},j} + \widetilde{M}_{i+\frac{1}{2},j-\frac{1}{2}} - \widetilde{L}_{i-\frac{1}{2},j+\frac{1}{2}} - L_{i-\frac{1}{2},j} - \widehat{L}_{i-\frac{1}{2},j-\frac{1}{2}}\right).
\end{aligned}$$

Observe from (3.16) that the energy fluxes cancel out in the telescopic sum and we obtain $\mathcal{T}_1 = 0$.

The second term $\mathcal{T}_2$ in (3.15) consists of numerical viscosity terms like

$$\mathcal{T}_{21} = \frac{|c|\Delta x}{4}\sum_{i,j} p_{i,j}\left(D_{-x}D_{+x}p_{i,j+1} + 2D_{-x}D_{+x}p_{i,j} + D_{-x}D_{+x}p_{i,j-1}\right). \tag{3.17}$$

Using summation by parts in (3.17) along with decay at infinity of p, we obtain

$$\mathcal{T}_{21} = -\frac{|c|\Delta x}{4}\left(\sum_{i,j} D_{+x}p_{i,j}D_{+x}p_{i,j+1} + 2\sum_{i,j}(D_{+x}p_{i,j})^2 + \sum_{i,j} D_{+x}p_{i,j}D_{+x}p_{i,j-1}\right)$$

$$= -\frac{|c|\Delta x}{2}\left(\sum_{i,j} D_{+x}p_{i,j}D_{+x}p_{i,j+1} + \sum_{i,j}(D_{+x}p_{i,j})^2\right) \quad \text{(by changing indices)}$$

$$\leq \frac{|c|\Delta x}{2}\left(\frac{1}{2}\sum_{i,j}(D_{+x}p_{i.j})^2 + \frac{1}{2}\sum_{i,j}(D_{+x}p_{i,j+1})^2 - \sum_{i,j}(D_{+x}p_{i,j})^2\right)$$

$$= 0.$$

The remaining terms in $\mathcal{T}_2$ can be treated analogously (we skip the details) to conclude that $\mathcal{T}_2 \leq 0$.

Summarizing the last two inequalities for $\mathcal{T}_1$ and $\mathcal{T}_2$, (3.15) yields

$$\frac{d}{dt}\sum_{i,j}\mathcal{E}_{i,j}(t) \leq 0,$$

and time integration leads to the energy bound (3.14). ∎

Remark 3.2. Theorem 3.2 shows that the symmetric potential-based scheme for the system wave equation is L^2-stable. A similar result holds for the diagonal potential-based scheme. The proof of L^2 stability relies on the fact that the underlying equations are linear and the question of their nonlinear entropy stability remains open. Nonlinear entropy stability will be proved for the related GMD isotropic scheme introduced in section 5.1.

4. Numerical experiments with vorticity preserving schemes. In this section, we will present several numerical experiments for illustrating the performance of the vorticity preserving symmetric and diagonal potential-based schemes. In particular, we consider the following schemes:

DS (DS2)	First-order (second-order) dimensional splitting with the Rusanov flux.
SYM (SYM2)	First-order (second-order) symmetric scheme (2.5).
SCP (SCP2)	First-order (second-order) vorticity preserving symmetric scheme (3.4) and (3.6).

The DS (DS2) scheme (see [19] for a detailed account of dimensional splitting) serves a reference scheme for comparing the numerical performance of the schemes designed in this paper. The vorticity preserving diagonal scheme (3.7) showed very similar behavior to SCP scheme and hence is omitted from the discussion below.

As noted before, the semidiscrete schemes are time integrated using the forward Euler method for the first-order schemes, and with a second-order strong stability preserving Runge–Kutta method [14], for second-order schemes. All the schemes use a standard Courant–Friedrichs–Levy (CFL) condition for determining the time stepping with a CFL number of 0.4.

4.1. Linear grad advection equations. We consider the two-dimensional linear grad advection equations (1.4) in the computational domain $[-2,2]\times[-2,2]$ with a given external velocity field,

$$(v_1, v_2) = (x, y).$$

The exact solution can be easily calculated as

$$\mathbf{u}(x,y,t) = R(t)\mathbf{u}_0(R(-t)(x,y)), \tag{4.1}$$

where $R(t)$ is a rotation matrix with angle t.

We consider curl free initial data:

$$\mathbf{u}_0(x,y) = 4\begin{pmatrix} -(y-\frac{1}{2}) \\ x \end{pmatrix} e^{-20\left((x)^2+(y-\frac{1}{2})^2\right)}. \tag{4.2}$$

The exact solution (4.1) is a smooth hump rotating about the origin and completing one rotation in time $t = 2\pi$. Nonreflecting Neumann type boundary conditions are used.

The solutions computed with the DS, SYM, SCP, and SCP2 schemes on a 100×100 mesh at time $t = 2\pi$ are shown in Figure 1. The quantity that is plotted is the norm: $\|u\| = \sqrt{u_1^2 + u_2^2}$. Clearly, the dimensional splitting (DS) scheme is inaccurate and the shape of the hump is destroyed. Furthermore, the scheme generates spurious waves that reach the boundary. Similarly, the symmetric scheme (2.5) is also inaccurate. On the other hand, the vorticity preserving version of the symmetric scheme (3.11) approximates the exact solution quite well. The shape of hump is preserved although the solution is diffused. Furthermore, the second-order SCP2 scheme provides a sharper resolution of the rotating hump. The second-order DS2 and SYM2 schemes are unstable in this case and the approximate solutions, generated by them, blow up at this time instant.

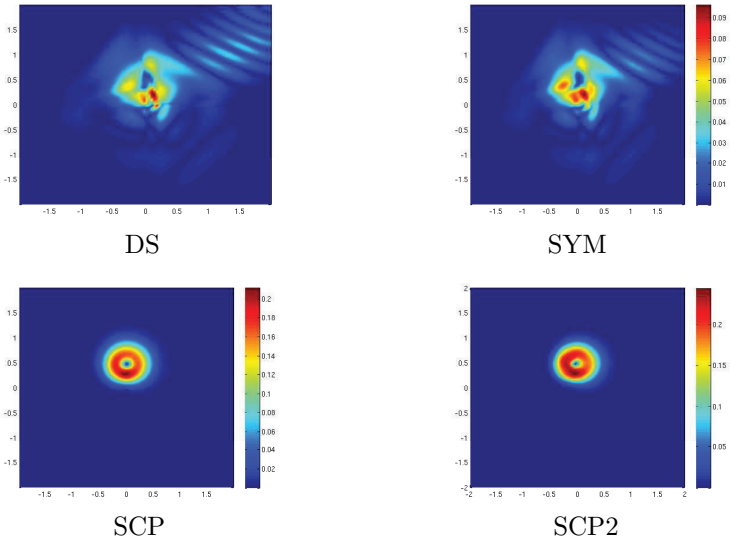

FIG. 1. *Approximate solutions computed with the DS, SYM, SCP, and SCP2 for numerical experiment for the linear grad advection* (1.4) *on a* 100×100 *mesh at time* $t = 2\pi$. *The quantity shown is the norm* $\|u\| = \sqrt{u_1^2 + u_2^2}$.

In order to compare the schemes and ascertain the cause of the above instabilities, we tabulate the errors in vorticity in Table 1. As shown in Lemma 3.1, the SCP and SCP2 scheme preserve the discrete vorticity (3.5a) to machine precision. The DS and SYM lead to vorticity errors which seem to be reducing with decreasing mesh size but both schemes blow up on a 400×400 mesh. Although the table does not provide conclusive evidence that preserving a discrete version of vorticity is essential for stability, the results suggest that only the vorticity preserving schemes can handle this test configuration.

Since the exact solution is known in this case, we calculate the errors in L^2 with the SCP and SCP2 schemes on a sequence of meshes. The results are shown in Figure

TABLE 1
Vorticity errors in L^2 for the linear grad advection equations (1.4).

M	DS	SYM	SCP	SCP2
50	1.8e-3	1.4e-3	6.2e-18	7.3e-18
100	4.9e-4	3.7e-4	5.0e-18	6.2e-18
200	4.9e-5	4.5e-5	3.8e-18	4.9e-18
400	blow up	blow up	3.0e-18	3.8e-18

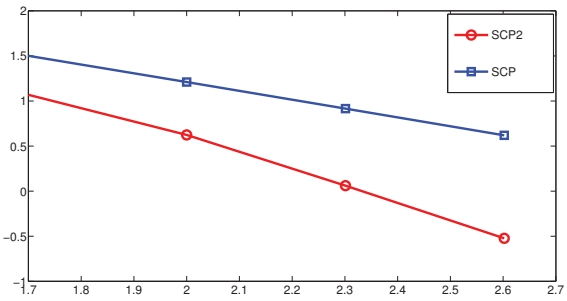

FIG. 2. *A log-log plot of the number of mesh points (x-axis) versus the relative error in L^2 (y-axis) for the linear grad advection* (1.4).

2. We see that the first-order SCP scheme has an experimental order of convergence of 1 and the second-order SCP scheme has an experimental order of convergence of approximately 1.92. Hence, the expected convergence rates are obtained with both schemes. This experiment clearly suggests that constraint (vorticity) preserving schemes are superior to standard schemes like DS and even to the vanilla version of the GMD symmetric scheme (2.5) if the latter is not properly tailored to preserve the vorticity-free constraint.

4.2. System wave equation. Following [20, 22], we consider the system wave equation (1.6) in the domain $[-2,2]\times[-2,2]$ with the initial data:

$$p(x,y,0) = -e^{-15(x^2+y^2)}, \qquad u_1(x,y,0) = u_2(x,y,0) \equiv 0. \tag{4.3}$$

The wave speed c in (1.6) is set to one. The initial data is smooth and the exact solution consists of smooth outward propagating circular waves. We compute on a uniform 200×200 mesh and recorded the approximate pressure and vorticity at time $t = 0.2$. In order to carefully compare the (minor) different schemes, we plot a slice (along the diagonal) of the DS(2), SYM(2), and SCP(2) schemes and compare them with a reference solution (computed with DS2 scheme on a mesh of 800×800 points) in Figure 3. The plot shows that among the first-order schemes, the vorticity preserving SCP scheme is slightly more accurate than the almost identical DS and SYM schemes. Among the second-order schemes, the SCP2 and SYM2 are clearly more accurate than the DS2 scheme which has an overshoot.

The initial data has zero vorticity and this is preserved in time. We tabulate the vorticity errors in L^2 for all the schemes in Table 2. As proved in Lemma 3.1, the SCP and SCP2 schemes preserve the vorticity. The DS and DS2 schemes show vorticity errors but these errors seem to decrease as the mesh is refined. Surprisingly, the SYM

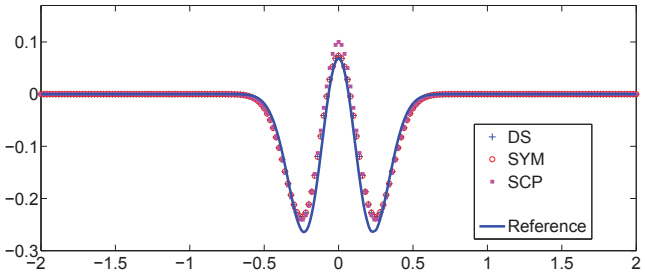

(a) 1st order

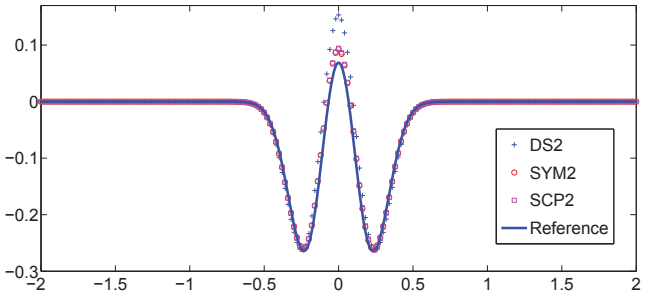

(b) 2nd order

FIG. 3. *A slice along the diagonal for p in the system wave equation. Comparison of all the schemes at* $t = 0.2$ *on a* 200×200 *mesh.*

TABLE 2
Vorticity errors in L^2 *for the system wave equations* (1.6).

M	DS	SYM	SCP	DS2	SYM2	SCP2
50	9.4e-5	1.2e-18	1.7e-18	8.8e-4	4.3e-4	1.8e-18
100	8.2e-6	5.3e-19	8.0e-19	1.5e-4	1.5e-4	1.1e-18
200	6.0e-7	2.6e-19	5.6e-19	2.0e-5	1.2e-5	7.6e-19
400	4.1e-8	1.4e-19	3.8e-19	2.3e-6	1.2e-6	4.9e-19

scheme also preserves vorticity in this case even though it is not designed to do so. However, this property is lost in the second-order version of the SYM scheme.

4.3. Nonlinear wave equation. We consider the nonlinear wave equation (1.7b) with nonlinearity $g(p) = \frac{1}{3}p^3$ in the domain $[-2, 2] \times [-2, 2]$ with the initial data (4.3). The choice of the cubic nonlinearity makes the system (1.7b) hyperbolic.

We compute on a uniform 100×100 mesh and plot a slice along the diagonal $x = y$ of the approximate pressure at time $t = 4.0$ in Figure 4. Even though the initial data is smooth, the solutions develop discontinuities in the form of shock waves. We use a reference solution computed with the second-order DS2 scheme on a 1000×1000 mesh. The results show that among the first-order schemes, the SCP is clearly more accurate than the SYM and DS scheme. The SYM2 and SCP2 schemes are slightly more accurate at the shocks than the DS2 schemes but have a slight overshoot behind the shock.

The errors in vorticity are tabulated in Table 3. They show that the SCP and

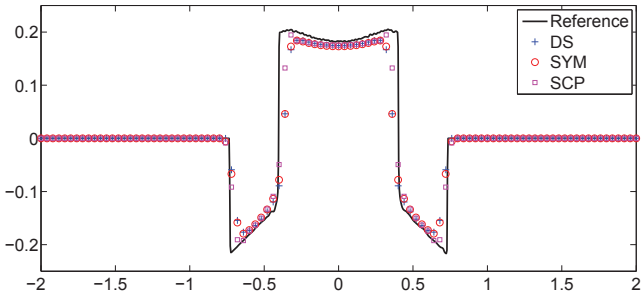

(a) 1st order

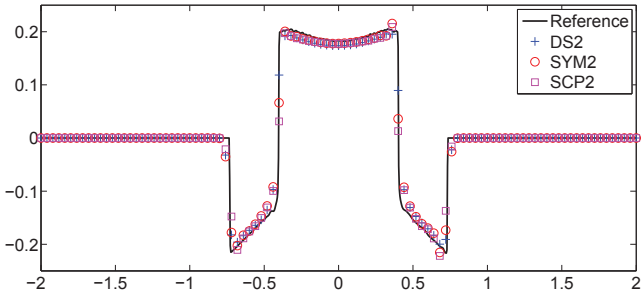

(b) 2nd order

FIG. 4. *A slice along the diagonal for p in the nonlinear wave equation. Comparison of all the schemes at* $t = 0.2$ *on a* 200×200 *mesh.*

TABLE 3
Vorticity errors in L^2 *for the nonlinear wave equations* (1.7b).

M	DS	SYM	SCP	DS2	SYM2	SCP2
50	2.9e-5	8.1e-6	7.7e-19	1.3e-4	1.0e-4	9.2e-18
100	9.6e-6	1.3e-6	6.7e-19	3.1e-5	3.5e-5	2.4e-18
200	2.7e-6	2.3e-7	4.8e-19	7.3e-6	6.5e-6	1.6e-19
400	7.8e-7	3.1e-8	3.6e-19	1.3e-6	1.2e-6	1.1e-19

SCP2 schemes preserve a discrete version of vorticity to machine precision whereas the SYM and DS scheme lead to small but converging vorticity errors. The SYM scheme has consistently lower vorticity errors than the DS scheme.

5. Genuinely multidimensional schemes—beyond constraint transport. The numerical experiments in the previous section show that the vorticity preserving schemes are superior to standard DS. A main feature of these potential-based schemes is their genuinely multidimensional (GMD) stencils (1.14) which enabled us to preserve the vorticity-free constraint in grad advection problems. More general systems of conservation laws (1.1) are not necessarily limited by any constraint transport, and it is therefore natural to examine the performance of GMD schemes on nonlinear problems *without* intrinsic constraints. We explore this issue in the context of the two-dimensional Euler equations of gas dynamics. We have three prototype examples of GMD schemes in mind. The first two are the class of potential-based schemes discussed in section 2: the symmetric schemes (2.5) and the diagonal schemes (2.6).

As a third example, we introduce below the class of *isotropic* GMD schemes: they are *not* rendered by a numerical potential but nevertheless highlight the use of a GMD stencil.

5.1. Isotropic GMD scheme. Let $\mathbf{F}(\cdot,\cdot)$ and $\mathbf{G}(\cdot,\cdot)$ be any two-point consistent numerical fluxes, and let $\mathbf{F}^{\pm},\mathbf{G}^{\pm}$ be the corresponding diagonal numerical fluxes in (2.6b). We define the isotropic fluxes

$$\begin{aligned}\widetilde{\mathbf{F}}_{i+\frac12,j} &:= \frac14\left(\mathbf{F}^{+}_{i+\frac12,j+\frac12}+2\mathbf{F}_{i+\frac12,j}+\mathbf{F}^{-}_{i+\frac12,j-\frac12}\right),\\ \widetilde{\mathbf{G}}_{i,j+\frac12} &:= \frac14\left(\mathbf{G}^{+}_{i+\frac12,j+\frac12}+2\mathbf{G}_{i,j+\frac12}+\mathbf{G}^{-}_{i-\frac12,j+\frac12}\right).\end{aligned} \tag{5.1a}$$

The resulting FV scheme reads as

$$\begin{aligned}\frac{d}{dt}\mathbf{U}_{i,j} &= -\frac{1}{\Delta x}\delta_x\widetilde{\mathbf{F}}_{i,j}-\frac{1}{Dy}\delta_y\widetilde{\mathbf{G}}_{i,j}\\ &= -\frac{1}{4\Delta x}\left(\delta_{/}\mathbf{F}^{+}_{i,j}+2\delta_x\mathbf{F}_{i,j}+\delta_{\backslash}\mathbf{F}^{-}_{i,j}\right)-\frac{1}{4\Delta y}\left(\delta_{/}\mathbf{G}^{+}_{i,j}+2\delta_y\mathbf{G}_{i,j}-\delta_{\backslash}\mathbf{G}^{-}_{i,j}\right);\end{aligned} \tag{5.1b}$$

here, $\delta_{/}$ and $\delta_{\backslash}$ denote the *diagonal* difference operators

$$\delta_{/}a_{I,J}:=a_{I+\frac12,J+\frac12}-a_{I-\frac12,J-\frac12},\quad \delta_{\backslash}a_{I,J}:=a_{I+\frac12,J-\frac12}-a_{I-\frac12,J+\frac12}. \tag{5.2}$$

The GMD structure of the scheme is clear from (5.1b): the scheme averages the fluxes along transverse directions. In contrast to the symmetric scheme (2.5), however, the explicit transverse information in (5.1b) is obtained by "rotating" the fluxes. Since the scheme (5.1b) takes into account all the directions in a cell, we term it as the *isotropic* GMD scheme.

The stencil of the isotropic scheme consists of nine points. Second-order accuracy can be obtained by the piecewise bilinear reconstruction (1.12). In addition to (1.13), we also need the corner point values

$$\begin{aligned}\mathbf{U}^{NE}_{i,j} &:= \mathbf{p}_{i,j}(x_{i+\frac12},y_{j+\frac12}),\quad \mathbf{U}^{NW}_{i,j} := \mathbf{p}_{i,j}(x_{i-\frac12},y_{j+\frac12}),\\ \mathbf{U}^{SE}_{i,j} &:= \mathbf{p}_{i,j}(x_{i+\frac12},y_{j-\frac12}),\quad \mathbf{U}^{SW}_{i,j} := \mathbf{p}_{i,j}(x_{i-\frac12},y_{j-\frac12}),\end{aligned} \tag{5.3a}$$

and the corresponding diagonal fluxes

$$\begin{aligned}\mathbf{F}^{+}_{i+\frac12,j+\frac12} &:= \mathbf{F}(\mathbf{U}^{NE}_{i,j},\mathbf{U}^{SW}_{i+1,j+1}),\quad \mathbf{F}^{-}_{i+\frac12,j-\frac12} := \mathbf{F}(\mathbf{U}^{SE}_{i,j},\mathbf{U}^{NW}_{i+1,j+1}),\\ \mathbf{G}^{+}_{i+\frac12,j+\frac12} &:= \mathbf{G}(\mathbf{U}^{NE}_{i,j},\mathbf{U}^{SW}_{i+1,j+1}),\quad \mathbf{G}^{-}_{i-\frac12,j+\frac12} := \mathbf{F}(\mathbf{U}^{NW}_{i,j},\mathbf{U}^{SE}_{i-1,j+1})\end{aligned} \tag{5.3b}$$

to define the second-order accurate version of the isotropic GMD scheme.

5.2. Stability analysis. The building blocks for the isotropic GMD schemes are standard FV fluxes $\mathbf{F},\mathbf{G}$. If these underlying fluxes are stable in a "suitable" sense, then we show that the resulting GMD scheme is stable. The stability study in this context will be based on the nonlinear *entropy stability* framework introduced by Tadmor in [32, 33, 34].

We assume that the system (1.1) is equipped with a convex entropy function $S(\mathbf{U})$ and compatible entropy fluxes $\eta=\eta(\mathbf{U}),\zeta=\zeta(\mathbf{U})$, such that solutions of (1.1) satisfy the entropy inequality

$$S(\mathbf{U})_t+\eta(\mathbf{U})_x+\zeta(\mathbf{U})_y\le 0. \tag{5.4}$$

The above inequality holds in the sense of distributions. The entropy inequality leads to stability estimates for the solution and provides a criteria for selecting physically meaningful solutions [8].

Let $\mathbf{V}(\mathbf{U}) := \partial_{\mathbf{U}}\eta$ be the vector of entropy variables and

$$\sigma := \langle \mathbf{V}, \mathbf{f}\rangle - \eta, \quad \tau := \langle \mathbf{V}, \mathbf{g}\rangle - \zeta$$

denote the *entropy potentials* associated with (1.1). The starting point of the entropy stability framework of [33] is the following.

DEFINITION 5.1 (entropy conservative fluxes). *The numerical fluxes* $\mathbf{F}^*_{i+\frac{1}{2},j}, \mathbf{G}^*_{i,j+\frac{1}{2}}$ *are termed entropy conservative if they satisfy*

$$\langle \delta_x \mathbf{V}_{i+\frac{1}{2},j}, \mathbf{F}^*_{i+\frac{1}{2},j}\rangle = \delta_x \sigma_{i+\frac{1}{2},j}, \quad \langle \delta_y \mathbf{V}_{i,j+\frac{1}{2}}, \mathbf{G}^*_{i,j+\frac{1}{2}}\rangle = \delta_y \tau_{i,j+\frac{1}{2}}. \tag{5.5}$$

Entropy conservative fluxes exist and can be written down explicitly [33, 34]. They can be used for a precise characterization of entropy stable schemes.

DEFINITION 5.2 (entropy stable fluxes [33]). *The numerical fluxes* $\mathbf{F}_{i+\frac{1}{2},j}, \mathbf{G}_{i,j+\frac{1}{2}}$ *are entropy stable if they admit the form*

$$\mathbf{F}_{i+\frac{1}{2},j} = \mathbf{F}^*_{i+\frac{1}{2},j} - Q_{i+\frac{1}{2},j}\delta_x \mathbf{V}_{i+\frac{1}{2},j}, \quad \mathbf{G}_{i,j+\frac{1}{2}} = \mathbf{G}^*_{i,j+\frac{1}{2}} - R_{i,j+\frac{1}{2}}\delta_y \mathbf{V}_{i,j+\frac{1}{2}}. \tag{5.6}$$

Here, $\mathbf{F}^*, \mathbf{G}^*$ *are some entropy conservative fluxes and* $Q = Q(\mathbf{U})$ *and* $R = R(\mathbf{U})$ *are strictly positive definite viscosity matrices with a constant* C *(independent of mesh size), such that for all vectors* $\mathbf{W}$

$$\min_{i,j}\{\langle \mathbf{W}, Q_{i+\frac{1}{2},j}\mathbf{W}\rangle,\ \langle \mathbf{W}, R_{i,j+\frac{1}{2}}\mathbf{W}\rangle\} \geq 0. \tag{5.7}$$

It was shown in [33] that any FV scheme (1.8) with *entropy stable* numerical fluxes $\mathbf{F}, \mathbf{G}$ satisfies a discrete version of the entropy inequality (5.4).

We extend the entropy stability results of [33] to the setting of the *isotropic* GMD scheme (5.1). To this end, we associate with the entropy conservative fluxes $\mathbf{F}^*$ and $\mathbf{G}^*$ in (5.5) and the corresponding *diagonal* entropy conservative fluxes $\mathbf{F}^{\pm,*}$ and $\mathbf{G}^{\pm,*}$, specified in (2.6b). The *diagonal* entropy stable fluxes are defined analogously. We have the following stability theorem.

THEOREM 5.3. *Consider the system of conservation laws* (1.1) *augmented with the entropy inequality* (5.4). *Assume that the numerical fluxes* $\mathbf{F}, \mathbf{G}$ *are entropy stable. Then the isotropic GMD scheme* (5.1) *based on these numerical fluxes is entropy stable, i.e., the isotropic approximate solutions* $\mathbf{U}_{i,j}$ *of* (5.1b) *satisfy the entropy stability estimate*

$$\frac{d}{dt}\sum_{i,j} S(\mathbf{U}_{i,j}(t)) \leq 0. \tag{5.8}$$

Proof. We modify the approach of [33] to the current setting. We multiply both sides of the isotropic GMD scheme (5.1b) by $\mathbf{V}_{i,j}$ to obtain

$$\begin{aligned}\frac{d}{dt}S(\mathbf{U}_{i,j}(t)) = &-\frac{1}{4\Delta x}\left(\langle \mathbf{V}_{i,j}, \delta_/ \mathbf{F}^+_{i,j}\rangle + 2\langle \mathbf{V}_{i,j}, \delta_x \mathbf{F}_{i,j}\rangle + \langle \mathbf{V}_{i,j}, \delta_\backslash \mathbf{F}^-_{i,j}\rangle\right)\\ &-\frac{1}{4\Delta y}\left(\langle \mathbf{V}_{i,j}, \delta_/ \mathbf{G}^+_{i,j}\rangle + 2\langle \mathbf{V}_{i,j}, \delta_y \mathbf{G}_{i,j}\rangle - \langle \mathbf{V}_{i,j}, \delta_\backslash \mathbf{G}^-_{i,j}\rangle\right) =: \mathcal{I} + \mathcal{II}.\end{aligned} \tag{5.9}$$

Denote the first term involving the inner product on the right-hand side of (5.9) as $\mathcal{I}_1 := \langle \mathbf{V}_{i,j}, \delta_/ \mathbf{F}^+_{i,j} \rangle$. Substituting the definition of an entropy stable flux $\mathbf{F}^+$ in (5.6) we have

$$\mathcal{I}_1 = \underbrace{\langle \mathbf{V}_{i,j}, \delta_/ \ \mathbf{F}^{+,*}_{i,j} \rangle}_{\mathcal{I}_{11}} - \underbrace{\Big(\langle \mathbf{V}_{i,j}, Q_{i+\frac12,j+\frac12} \delta_/ \mathbf{V}_{i+\frac12,j+\frac12} \rangle - \langle \mathbf{V}_{i,j}, Q_{i-\frac12,j-\frac12} \delta_/ \mathbf{V}_{i-\frac12,j-\frac12} \rangle \Big)}_{\mathcal{I}_{12}}.$$

We consider the terms $\mathcal{I}_{11}$ and $\mathcal{I}_{12}$ separately. Using the straightforward identity

$$\mathbf{V}_{i,j} \equiv \mu_/ \mathbf{V}_{i+\frac12,j+\frac12} - \frac12 \delta_/ \mathbf{V}_{i+\frac12,j+\frac12}, \qquad \mu_/ a_{I,J} := \frac{a_{I+\frac12,J+\frac12} + a_{I-\frac12,J-\frac12}}{2}, \tag{5.10}$$

we obtain

$$\begin{aligned} \mathcal{I}_{11} = & \Big\langle \mu_/ \mathbf{V}_{i+\frac12,j+\frac12}, \mathbf{F}^{+,*}_{i+\frac12,j+\frac12} \Big\rangle - \Big\langle \mu_/ \mathbf{V}_{i-\frac12,j-\frac12}, \mathbf{F}^{+,*}_{i-\frac12,j-\frac12} \Big\rangle \\ & - \frac12 \Big\langle \delta_/ \mathbf{V}_{i+\frac12,j+\frac12}, \mathbf{F}^{+,*}_{i+\frac12,j+\frac12} \Big\rangle - \frac12 \Big\langle \delta_/ \mathbf{V}_{i-\frac12,j-\frac12}, \mathbf{F}^{+,*}_{i-\frac12,j-\frac12} \Big\rangle. \end{aligned}$$

Now, in view of the entropy conservation relation $\big\langle \delta_/ \mathbf{V}_{i+\frac12,j+\frac12}, \mathbf{F}^{+,*}_{i+\frac12,j+\frac12} \big\rangle = \delta_/ \sigma_{i+\frac12,j+\frac12}$, we have

$$\mathcal{I}_{11} = \Big\langle \mu_/ \mathbf{V}_{i+\frac12,j+\frac12}, \mathbf{F}^{+,*}_{i+\frac12,j+\frac12} \Big\rangle - \langle \mu_/ \mathbf{V}_{i-\frac12,j-\frac12}, \mathbf{F}^{+,*}_{i-\frac12,j-\frac12} \rangle - \frac12 \delta_/ \sigma_{i+\frac12,j+\frac12} - \frac12 \delta_/ \sigma_{i-\frac12,j-\frac12},$$

and simple algebraic manipulations finally yield

$$\mathcal{I}_{11} = \Big\langle \mu_/ \mathbf{V}_{i+\frac12,j+\frac12}, \mathbf{F}^{+,*}_{i+\frac12,j+\frac12} \Big\rangle - \Big\langle \mu_/ \mathbf{V}_{i-\frac12,j-\frac12}, \mathbf{F}^{+,*}_{i-\frac12,j-\frac12} \Big\rangle - \mu_/ \sigma_{i+\frac12,j+\frac12} + \mu_/ \sigma_{i-\frac12,j-\frac12}.$$

Using the same identity (5.10) in the numerical viscosity term $\mathcal{I}_{12}$, we obtain

$$\begin{aligned} \mathcal{I}_{12} = & \Big\langle \mu_/ \mathbf{V}_{i+\frac12,j+\frac12}, Q_{i+\frac12,j+\frac12} \delta_/ \mathbf{V}_{i+\frac12,j+\frac12} \Big\rangle - \Big\langle \mu_/ \mathbf{V}_{i+\frac12,j+\frac12}, Q_{i-\frac12,j-\frac12} \delta_/ \mathbf{V}_{i-\frac12,j-\frac12} \Big\rangle \\ & - \frac12 \Big\langle \delta_/ \mathbf{V}_{i+\frac12,j+\frac12}, Q_{i+\frac12,j+\frac12} \delta_/ \mathbf{V}_{i+\frac12,j+\frac12} \Big\rangle - \frac12 \Big\langle \mu_/ \mathbf{V}_{i+\frac12,j+\frac12}, Q_{i-\frac12,j-\frac12} \delta_/ \mathbf{V}_{i-\frac12,j-\frac12} \Big\rangle. \end{aligned}$$

Define the consistent numerical flux

$$\begin{aligned} \eta^+_{i+\frac12,j+\frac12} := & \Big\langle \mu_/ \mathbf{V}_{i+\frac12,j+\frac12}, \mathbf{F}^{+,*}_{i+\frac12,j+\frac12} \Big\rangle - \mu_/ \sigma_{i+\frac12,j+\frac12} \\ & - \Big\langle \mu_/ \mathbf{V}_{i+\frac12,j+\frac12}, Q_{i+\frac12,j+\frac12} \delta_/ \mathbf{V}_{i+\frac12,j+\frac12} \Big\rangle. \end{aligned}$$

Straightforward calculations then yield

$$\begin{aligned} \mathcal{I}_1 = \mathcal{I}_{11} - \mathcal{I}_{12} = & \delta_/ \eta^+_{i,j} + \frac12 \Big\langle \delta_/ \mathbf{V}_{i+\frac12,j+\frac12}, Q_{i+\frac12,j+\frac12} \delta_/ \mathbf{V}_{i+\frac12,j+\frac12} \Big\rangle \\ & + \frac12 \Big\langle \delta_/ \mathbf{V}_{i+\frac12,j+\frac12}, Q_{i-\frac12,j-\frac12} \delta_/ \mathbf{V}_{i-\frac12,j-\frac12} \Big\rangle \\ \geq & \ \delta_/ \eta^+_{i,j}. \end{aligned} \tag{5.11}$$

This provides the entropy stability estimate on the first term on the right-hand side of (5.9). Similarly, the entropy stability of the second and third terms in the expression $\mathcal{I}$ in (5.9) is verified using the corresponding entropy fluxes

$$\eta_{i+\frac12,j} := \Big\langle \mu_/ \mathbf{V}_{i+\frac12,j}, \mathbf{F}^*_{i+\frac12,j} \Big\rangle - \mu_/ \sigma_{i+\frac12,j} - \Big\langle \mu_/ \mathbf{V}_{i+\frac12,j}, Q_{i+\frac12,j} \delta_/ \mathbf{V}_{i+\frac12,j} \Big\rangle,$$

$$\eta^-_{i+\frac12,j-\frac12} := \left\langle \mu_/ \mathbf{V}_{i+\frac12,j-\frac12}, \mathbf{F}^{-,*}_{i+\frac12,j-\frac12} \right\rangle - \mu_/ \sigma_{i+\frac12,j-\frac12} - \left\langle \mu_/ \mathbf{V}_{i+\frac12,j-\frac12}, Q_{i+\frac12,j-\frac12} \delta_/ \mathbf{V}_{i+\frac12,j\frac12} \right\rangle.$$

The rest of the terms in (5.9) grouped under $\mathcal{II}$ can be manipulated in a similar manner, using consistent numerical entropy fluxes $\zeta, \zeta^{\pm}$ which are defined analogously. We end up with the following discrete entropy inequality:

(5.12)
$$\frac{d}{dt} S(\mathbf{U}_{i,j}(t)) \le -\frac{1}{4\Delta x}\left(\delta_/ \eta^+_{i,j} + 2\delta_x \eta_{i,j} + \delta_\backslash \eta^-_{i,j}\right) - \frac{1}{4\Delta y}\left(\delta_/ \zeta^+_{i,j} + 2\delta_y \zeta_{i,j} - \delta_\backslash \zeta^-_{i,j}\right).$$

Summing (5.12) over i, j, we obtain the entropy stability estimate (5.8). ∎

Remark 5.1. Observe that if we use the entropy *conservative* fluxes $\mathbf{F}^*, \mathbf{G}^*$, then the corresponding isotropic GMD scheme (5.1) with $\widetilde{\mathbf{F}^*}$ and $\widetilde{\mathbf{G}^*}$ is, in fact, entropy conservative.

5.3. Numerical experiments with Euler equations. We consider the two-dimensional Euler equations [18] with two types of initial data.

Radially symmetric data. The Euler equations are considered subject to the two-dimensional initial data

(5.13)
$$\rho(x,y,0) = p(x,y,0) = \begin{cases} 1.0 & \text{if} \quad \sqrt{x^2+y^2} < 0.4, \\ 0.125 & \text{otherwise}, \end{cases}$$
$$u(x,y,0) = v(x,y,0) \equiv 0.$$

Here ρ is the density, (u, v) is the velocity field, and p is the pressure. The initial radial discontinuity breaks into three radially symmetric waves: an outward propagating shock wave, a contact discontinuity, and a rarefaction wave. We consider the computational domain $[-1, 1] \times [-1, 1]$ and show a one-dimensional slice of the computed density along the diagonal $x = y$ at time $t = 0.2$. The results shown in Figure 5 are computed on a 100×100 mesh with DS(2) and SYM(2) schemes. Furthermore, we also show the results with the isotropic GMD scheme (5.1b) under the label ISO(2) scheme. For the sake of comparison, a reference solution computed with a second-order DS2 scheme on a 1000×1000 mesh is also shown. The results indicate that the SYM and ISO schemes are comparable to the DS scheme. There are very minor differences between these three schemes. The second-order schemes are clearly more accurate than the first-order schemes. The SYM2 scheme shows slight oscillations behind the shock but the ISO2 scheme is virtually identical with the DS2 scheme.

Two-dimensional Riemann problem. The Euler equations are considered together with the two-dimensional Riemann initial data

(5.14)
$$\begin{aligned} \rho = 1.1, \quad u = 0, \quad v = 0, \quad p = 1.1 \quad &\text{if} \quad x > 0, y > 0, \\ \rho = 0.5065, \quad u = 0, \quad v = 0.8939, \quad p = 0.35 \quad &\text{if} \quad x > 0, y < 0, \\ \rho = 0.5065, \quad u = 0.8939, \quad v = 0, \quad p = 0.35 \quad &\text{if} \quad x < 0, y > 0, \\ \rho = 1.1, \quad u = 0.8939, \quad v = 0.8939, \quad p = 1.1 \quad &\text{if} \quad x < 0, y < 0. \end{aligned}$$

The exact solution [31, 19, 21] consists of two forward moving shocks and two backward moving shocks. The computational domain is $[-1, 1]\times[-1, 1]$. A one-dimensional slice of the approximate density along the line $x = -y$ at time $t = 0.25$ is shown in Figure 6. The results are very similar to the previous experiment. The DS, SYM, and ISO schemes are comparable in their resolution. All of them being far more diffusive

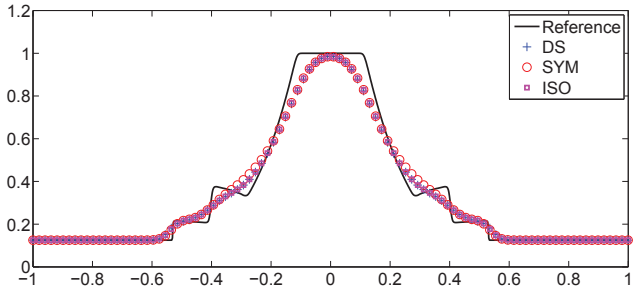

(a) 1st order

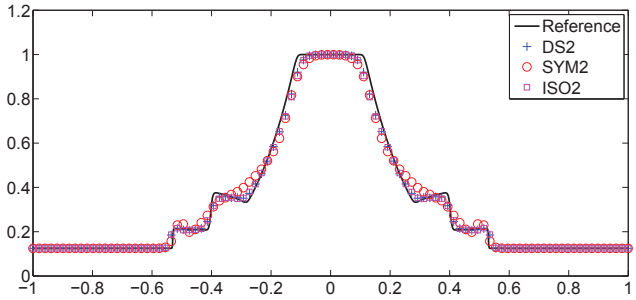

(b) 2nd order

FIG. 5. *A slice of the computed density along the diagonal $x = y$ for the Euler equations with radially symmetric data* (5.13). *Results are for the $DS(2)$, $SYM(2)$, and $ISO(2)$ schemes at time $t = 0.2$ on a 100×100 mesh.*

than the second-order schemes. There are very minor differences between the DS2, SYM2, and ISO2 schemes in this case.

Remark 5.2. The GMD schemes are designed to resolve flows involving strong interaction between the normal and transverse directions. Hence, these schemes may not be as accurate as genuinely multidimensional schemes like those designed in [1, 10, 19, 20] in resolving situations like strong shear flows where information in one direction dominates.

6. Conclusion. We consider multidimensional conservation laws equipped with intrinsic constraints. In particular, we consider equations that include grad advection (1.2) as a component. The constraint of interest is the vorticity (curl of the solution field). Examples include the linear grad advection equations (1.4), the system wave equation (1.6), and a nonlinear wave equation (1.7b).

We design vorticity preserving numerical schemes for approximating these equations. The design involves a two-step procedure. In the first step, a standard FV scheme is reformulated in terms of vertex centered numerical potentials. *Any* consistent FV flux can be used to define potentials. This construction leads to GMD schemes that incorporate explicit transverse information. One such scheme, the isotropic GMD scheme, is shown to be entropy stable. Numerical experiments with the Euler equations show that these schemes are comparable to the DS procedure in terms of numerical performance.

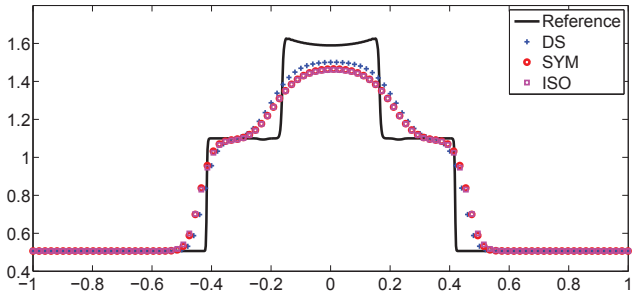

(a) 1st order

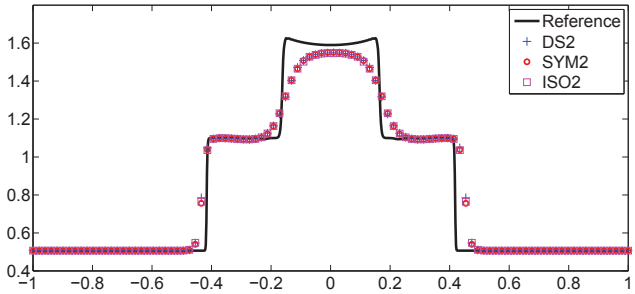

(b) 2nd order

FIG. 6. *A slice of the computed density along the line* $x = -y$ *for the Euler equations with Riemann initial data* (5.14). *Results are for the* $DS(2)$, $SYM(2)$, *and* $ISO(2)$ *schemes at time* $t = 0.5$ *on a* 100×100 *mesh.*

Moreover, the potential-based fluxes serve as a basis for the construction of vorticity preserving schemes. These schemes, constructed by a suitable choice of the numerical potentials, are shown to preserve a discrete version of the vorticity. Furthermore, we show that vorticity preserving schemes for the system wave equation are energy stable. The schemes presented here are similar in spirit to those proposed in recent papers [23] and [24] for preserving discrete divergence in the magnetic induction equations and the MHD equations, respectively.

Numerical experiments for linear grad advection equations, the system wave equation, and a nonlinear wave equation are presented. They clearly demonstrate the superior performance of the constraint preserving schemes compared to standard approaches like dimensional splitting.

Acknowledgments. The work on this paper began when S. M. visited the Center of Scientific Computation and Mathematical Modeling (CSCAMM) and he thanks CSCAMM and all its members for the excellent hospitality and facilities. E. T. thanks the Centre for Advanced Study at the Norwegian Academy of Science and Letters for hosting him as part of its international research program on Nonlinear PDEs during the academic year 2008–2009.

REFERENCES

[1] R. Abgrall and P. L. Roe, *High order fluctuation schemes on triangular meshes*, J. Sci. Comput., 19 (2003), pp. 3–36.

[2] J. Bálbas, E. Tadmor, and C. C. Wu, *Non-oscillatory central schemes for one and two-dimensional magnetohydrodynamics*, I, J. Comput. Phys., 201 (2004), pp. 261–285.

[3] D. S. Balsara and D. Spicer, *A staggered mesh algorithm using high order Godunov fluxes to ensure solenoidal magnetic fields in magnetohydrodynamic simulations*, J. Comput. Phys., 149 (1999), pp. 270–292.

[4] S. J. Billett and E. F. Toro, *On WAF-type schemes for multidimensional hyperbolic conservation laws*, J. Comput. Phys., 130 (1997), pp. 1–24.

[5] J. U. Brackbill and D. C. Barnes, *The effect of nonzero $\nabla \cdot B$ on the numerical solution of the magnetohydrodynamic equations*, J. Comput. Phys., 35 (1980), pp. 426–430.

[6] A. J. Chorin, *Numerical solutions of the Navier-Stokes equations*, Math. Comp., 22 (1968), pp. 745–762.

[7] P. Colella, *Multi-dimensional upwind methods for hyperbolic conservation laws*, J. Comput. Phys., 87 (1990), pp. 171–200.

[8] C. Dafermos, *Hyperbolic Conservation Laws in Continuum Physics*, Springer, Berlin, 2009.

[9] W. Dai and P. R. Woodward, *A simple finite difference scheme for multidimensional magnetohydrodynamic equations*, J. Comput. Phys., 142 (1998), pp. 331–369.

[10] H. Deconnik, P. L. Roe, and R. Struijs, *A multi-dimensional generalization of Roe's flux difference splitter for Euler equations*, Comput. Fluids, 22 (1993), pp. 215–222.

[11] M. Fey, *Multidimensional upwinding.* I. *The method of transport for solving the Euler equations*, J. Comput. Phys., 143 (1998), pp. 159–180.

[12] M. Fey, *Multidimensional upwinding.* II. *Decomposition of Euler equations into advection equations*, J. Comput. Phys., 143 (1998), pp. 181–199.

[13] F. G. Fuchs, A. D. McMurry, S. Mishra, N. H. Risebro, and K. Waagan, *Approximate Riemann solvers and robust high order finite volume schemes for multi-dimensional ideal MHD equations*, Commun. in Comput. Phys., 9 (2011), pp. 324–362.

[14] S. Gottlieb, C.-W. Shu, and E. Tadmor, *Strong stability-preserving high-order time discretization methods*, SIAM Rev., 43 (2001), pp. 89–112.

[15] A. Harten, B. Engquist, S. Osher, and S. R. Chakravarty, *Uniformly high-order accurate essentially nonoscillatory schemes*, III, J. Comput. Phys., 71 (1987), pp. 231–303.

[16] R. Jeltsch and M. Torrilhon, *On curl-preserving finite volume discretizations for shallow water equations*, BIT, 46 (2006), suppl. pp. 535–553.

[17] A. Kurganov and E. Tadmor, *New high-resolution central schemes for nonlinear conservation laws and convection-diffusion equations*, J. Comput. Phys, 160 (2000), pp. 241–282.

[18] R. J. LeVeque, *Finite Volume Methods for Hyperbolic Problems*, Cambridge University Press, Cambridge, UK, 2002.

[19] R. J. LeVeque, *Wave propagation algorithms for multi-dimensional hyperbolic systems*, J. Comput. Phys., 131 (1997), pp. 327–353.

[20] M. Lukáčová-Medvidóvá, K. W. Morton, and G. Warnecke, *Evolution Galerkin methods for Hyperbolic systems in two space dimensions*, Math. Comp., 69 (2000), pp. 1355–1384.

[21] M. Lukáčová-Medvidóvá, J. Saibertova, and G. Warnecke, *Finite volume evolution Galerkin methods for nonlinear hyperbolic systems*, J. Comput. Phys., 183 (2002), pp. 533–562.

[22] M. Lukáčová-Medvidóvá and J. Saibertova, *Finite volume schemes for multi-dimensional hyperbolic systems based on use of bicharacteristics*, Appl. Math., 51 (2006), pp. 205–228.

[23] S. Mishra and E. Tadmor, *Constraint preserving schemes using potential-based fluxes.* I. *Multidimensional transport equations*, Commun. Comput. Phys., 9 (2010), pp. 688–710.

[24] S. Mishra and E. Tadmor, *Constraint preserving schemes using potential-based fluxes.* III. *Genuinely multi-dimensional schemes for the MHD equations*, M2AN Math. Model. Numer. Anal., to appear.

[25] K. W. Morton and P. L. Roe, *Vorticity preserving Lax–Wendroff type schemes for the system wave equation*, SIAM J. Sci. Comput., 23 (2001), pp. 170–192.

[26] H. Nishikawa and P. L. Roe, *Towards high-order fluctuation-splitting schemes for Navier-Stokes equations*, 17th AIAA CFD Conference, 2005-5244, Toronto, Ontario, 2005.

[27] S. Noelle, *The MOT-ICE: A new high-resolution wave propagation algorithm for multi-dimensional systems of conservation laws based on Fey's method of transport*, J. Comput. Phys., 164 (2000), pp. 283–334.

[28] K. G. Powell, *An Approximate Riemann Solver for Magneto-hydro Dynamics (That Works in More Than One Space Dimension)*, Technical report 94-24, ICASE, Langley, VA, 1994.

[29] D. S. Ryu, F. Miniati, T. W. Jones, and A. Frank, *A divergence free upwind code for multidimensional magnetohydrodynamic flows*, Astrophys. J., 509 (1998), pp. 244–255.
[30] C. W. Shu and S. Osher, *Efficient implementation of essentially nonoscillatory schemes*. II, J. Comput. Phys., 83 (1989), pp. 32–78.
[31] C. W. Schulz-Rinne, J. P. Collins, and H. M. Glaz, *Numerical solution of the Riemann problem for two-dimensional gas dynamics*, SIAM J. Sci. Comput., 14 (1993), pp. 1394–1414.
[32] E. Tadmor, *Numerical viscosity and entropy conditions for conservative difference schemes*, Math. Comp., 43 (1984), pp. 369–381.
[33] E. Tadmor, *The numerical viscosity of entropy stable schemes for systems of conservation laws*, I, Math. Comp., 49 (1987), pp. 91–103.
[34] E. Tadmor, *Entropy stability theory for difference approximations of nonlinear conservation laws and related time-dependent problems*, Acta Numer., 12 (2003), pp. 451–512.
[35] E. Tadmor, *Approximate solutions of nonlinear conservation laws*, in Advanced Numerical approximations of Nonlinear Hyperbolic Equations, A. Quarteroni ed., Lecture Notes in Math. 1697, Springer, Berlin, 1998, pp. 1–149.
[36] M. Torrilhon, *Locally divergence-preserving upwind finite volume schemes for magnetohydrodynamics*, SIAM J. Sci. Comput., 26 (2005), pp. 1166–1191.
[37] M. Torrilhon and M. Fey, *Constraint-preserving upwind methods for multidimensional advection equations*, SIAM J. Numer. Anal., 42 (2004), pp. 1694–1728.
[38] G. Toth, *The $\nabla \cdot B = 0$ constraint in shock capturing magnetohydrodynamics codes*, J. Comp. Phys., 161 (2000), pp. 605–652.